Journal of Applied Fluid Mechanics, Vol. 4, No. 2, Special Issue, pp. 81-87, 2011.
Available online at www.jafmonline.net, ISSN 1735-3572, EISSN 1735-3645.
DOI: 10.36884/jafm.4.03.11937

Experimental and Numerical Investigations of Two-Phase Electrolysis Processes - Electrical Energy Conversion in Hydrogen Production

Z. Derhoumi[1], P. Mandin[1†], R. Wuthrich[2] and H. Roustan[3]

[1] *LIMatB EA4250, Université de Bretagne Sud, Centre de recherche rue de Saint-Maudé, 56100 Lorient, France*
[2] *Department of Mechanical & Industrial Engineering, Concordia University, 1455 de Maisonneuve Blvd. West, Montreal, Quebec, H3G 1M8 Canada*
[3] *Alcan – Centre de Recherche de Voreppe -725 rue Aristide Bergès - BP 27 – 38341 Voreppe Cedex, France*

†*Corresponding Author Email: philippe.mandin@univ-ubs.fr*

(Received April 25, 2010; accepted March 13, 2011)

ABSTRACT

During two-phase electrolysis processes, for example for hydrogen production, there are bubbles which are created at electrodes. This implies a great vertical motion source in the normal earth gravity field and then a quite important natural two-phase convection. All other fields are then affected. Heat, mass and electricity transfers are modified due to both bubbles screening (at surface and in volume) and to bubbles transport promotion. Many numerical modeling for two-phase processes such as kerosene pulverization in engines or coal combustion sciences have shown the difficulties of these multi-physics processes. Both particles and reactor scales must be considered according with a strong coupling modeling. In these processes the particles injection is "in the flow". In boiling or electrolysis processes, a new difficulty is added: particles birth or injection is strongly coupled to the local flow properties and leads to a complex boundary condition at surfaces. Electrical and electrochemical properties and processes are disturbed. This disturbance can lead to the modification of the local current density and to anode effects for example. There is few works concerning the local modelling of electrochemical processes during a two-phase electrolysis process. There are also few local experimental measurements in term of chemical composition, temperature or current density which will allow the numerical calculations validation. The present work shows the started numerical modeling strategy and the first results, both experimental and numerical obtained.

Keywords: Two-phase, Electrochemical, Processes, Modelling.

NOMENCLATURE

j	Current density (A m^{-2})
V	Velocity (m s^{-1})
P	Pressure (Pa)
A	Area of electrode (m²)
C	Concentration
T	Temperature (K)
h	*Heat transfer coefficient*
D	*Diffusion coefficient*
F	*Fraction*
R	*Particle radius* (m)
C_p	Specific heat (J kg^{-1} K^{-1})
k	Mass transfer coefficient

Greek letters

Θ	Average bubble coverage
λ	Thermal conductivity (W m^{-1} K^{-1})
γ	Capillarity
ρ	Mass of volume (kg m^{-3})
σ	Electrical conductivity (S m^{-1})
ν	kinetic viscosity (m² s^{-1})
μ	Dynamic viscosity (kg m^{-1} s^{-1})

Subscripts

C	Critical
D	Drag
L	Liquid
G	Gas

1. INTRODUCTION

During the two-phase electrolysis processes of aluminium, Fluorine and hydrogen production, the imposed electrical energy leads to the electrochemical reaction at electrodes followed by a gaseous release which modifies the electric properties of the electrolysis. Furthermore, growth and departure of bubbles from the wall of electrode induce a microconvection controlling the mass transfer coefficient. In all cases of two-phase electrolysis cited, a portion of the electrode surface is covered by bubbles which significantly decrease the available mass transfer surface because of screening.

The analogy between heat and mass transfer allows the use of Chilton-Colburn analogy. This analogy is beneficial particularly for research in gas-evolving electrode since the process in boiling has been exhaustively studied and also better understood than the process in gas evolution for a two-phase electrolysis. Using this analogy is justified because both processes of the evolution of the gas and the boiling are the resultant of transport. The modelling of the electrochemical cell performances needs the use of numerical calculation at two different scales (bubble and electrochemical cell) strongly coupled. Then, for both boiling and two-phase electrolysis processes modelling, it is necessary to perform the numerical simulation of the flow and mass transport around a bubble. The obtained information must then be integrated in a macroscopic scale modelling. The modelling of gas release leads to consider chemical, electrical, hydrodynamic and electrochemical phenomena because a bubble is a source of momentum which induces a strong coupling of hydrodynamic properties and mass transfer phenomena and also of scales.

During the two-phase electrolysis, bubble population increases with the current density. The local current density j is related to the average current density I/A and the average bubble coverage Θ given by Wuthrich (2004)

$$j = \frac{I/A}{1-\Theta} \tag{1}$$

When operating a two-phase electrolysis, a fraction Fg of the dissolved gas in the solution is transported to liquid - gas interface of adhering bubbles and is there transformed into the gaseous phase (Fig. 1). The fraction (1-Fg) is transported far from the electrode to the bulk but can also contribute to the small growth of freely moving bubbles. The relation between the fraction of dissolved gas transported in bubbles and the average coverage Θ is given by Vogt (2003):

$$Fg = 1-(1-\Theta)^{2.5} \tag{2}$$

With

$$\Theta = 0.023\left(\frac{I}{A}\right)^{0.3} \tag{3}$$

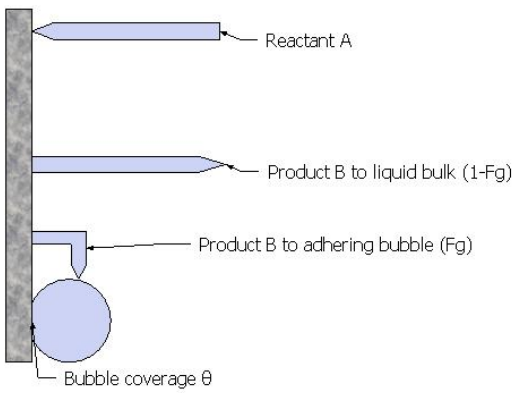

Fig. 1. The schematic representation of the bubbles formation during a two-phase electrolysis.

When the current intensity increases, the average coverage bubble increases and the fraction Fg transported to the adhering bubbles decreases which prevents bubbles to reaching the critical radius of nucleation Rc given by Vogt (2003):

$$R_c = \frac{2\gamma}{P_g - P_l} \tag{4}$$

The nucleation of bubbles occurs if the condition R>Rc is validated (Fig. 2).

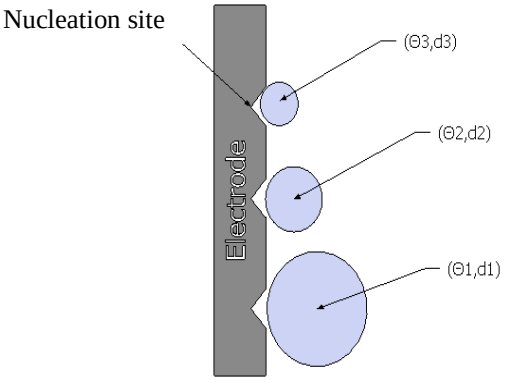

Fig. 2. Graphical illustration of the bubbles nucleation.

Using the Chilton-Colburn analogy between mass transfer and heat simplifies the problem because instead of solving the equation of species conservation (mass transfer), it solves the heat equation (heat transfer) studied extensively.The problem of mass transfer is described by the equation of species conservation:

$$\partial C/\partial t - D\Delta C = 0 \tag{5}$$

The problem of heat transfer is described by the heat equation.

$$\partial T/\partial t - D_T\Delta T = 0 \text{ with } D_T = \lambda/(\rho.C_P) \tag{6}$$

The heat equation is identical as the one of species conservation. The analogy between these equations is due to:

1/ the similarity of the Schmidt number $Sc = \upsilon / D$ with the Prandtl one;

2/ the similarity of the Sherwood number with the Nusselt number:

$$Sh = \frac{kd}{D} \tag{7}$$

The Chilton–Colburn Analogy for heat and mass transfer gives the relationship between the heat and mass transfer. The Chilton-Colburn factor for heat transfer is given by:

$$J_H = \frac{h}{\rho v C_p}\mathrm{Pr}^{2/3} \tag{8}$$

The Chilton Colburn factor for mass transfer is given by:

$$J_D = \frac{k}{v}Sc^{2/3} \tag{9}$$

Thus for the laminar boundary layer over a spherical particle

$$J_D = J_H \quad \Leftrightarrow \quad \frac{\mathrm{h}}{\rho v C_p}\mathrm{Pr}^{2/3} = \frac{k}{v}Sc^{2/3} \qquad (10)$$

This equation is considered valid for liquid and gases within the ranges 0.6<Sc<2500 and 0.6<Pr<100. They have been observed to be a reasonable approximation for various geometries, such as flow over a spherical particle.

2. EXPERIMENTAL SET-UP AND CONDITIONS

2.1 Description

To estimate and observe experimentally the intrinsic properties of the bubbles nucleation and growth, the electrochemically induced flow in the gravity field is a problem. The two-phase boundary layer is difficult to describe. The induced flow due to Archimede forces is cell geometry dependent. So, in the goal to identify bubbles wettability intrinsic properties, It has been decided to complete the in lab normal gravity, measurements with zero gravity experiments.

Observation and measurements of two-phase electrolysis processes with bubbles production and gas–evolving processus in different conditions of gravity have been made. During those experiments in laboratory (presence of gravity) it has been observed some convective micro-exchange on the scale of bubbles and macro-convection on the scale of the electrolysis cell. These exchanges prevent the intrinsic triplet "gas – liquid electrolyte – solid electrode" properties identification. In the same conditions, bubbles have been extracted by the Archimede forces and hydrodynamic friction of the natural flow and thus have a size in normal gravity smaller than in zero gravity condition. The experiences in zero gravity condition have been made aboard the Novespace® Airbus A300 plane. To obtain the zero gravity condition in electrochemical cells, the plane follows parabolic trajectories.

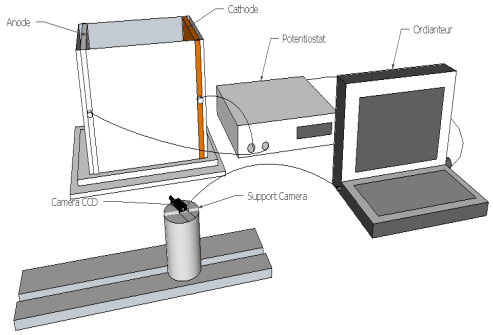

Fig. 3. The experimental dispositif used in labratory

The experimental work in zero gravity consists to perform electrolysis and chronopotentiometry with a potentiostat and observe by video (CCD and camescope) and measure the bubble formation and growth without natural convection.

These measures will allow the identification of the processes properties and the development of a multi-physical model of the bubbles growth and the gaseous release which defines the two-phase electrode boundary layer.

2.2 Measurements

The bubble diameter evolution measurements during the experiments requires the electrolysis images processing and analysis. This operation consists to use a Java program (Macro image processing) as shown in Fig. 5.

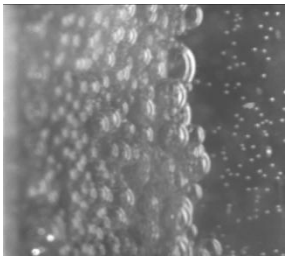

Fig. 4. Bubbles layer Photography

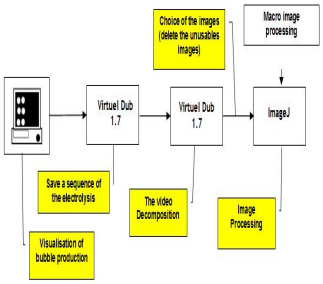

Fig. 5. Image processing schema

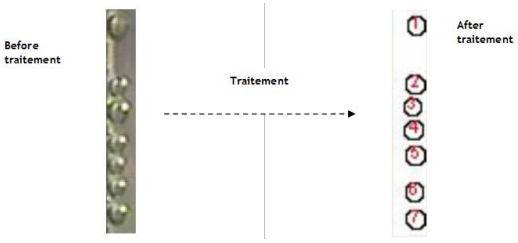

Fig. 6. Bubble image (before and after treatment)

Table 1 gives performed experiments definition. The image processing allows the calculation of the bubble diameter evolution during the different periods of experiment.

Table 1 Experiment data

Parabole	phase	Time (s)	Intensity (A)	Cell /solution	Anode/Cathode	Cell n°
Prabole1	0G	26 - 45	0.1	Na2SO4 115,6g/L CuSO4 13,3g/L	Ni/Cu	1
	1.8G.Before	0 - 26				
	1.8G. After	45 - 68				
Parabole26	0G	24 - 45	0.3	Na2SO4 115,6g/L CuSO4 13,3g/L	Ni/Cu	1
	1.8G.Before	0 - 24				
	1.8G. After	45 - 70				
Prabole3	0G	23 - 44	0.15	Na2SO4 115,6g/L CuSO4 13,3g/L	Ni/Cu	1
	1.8G.Before	0 - 23				
	1.8G. After	44 - 70				

The Fig. 7 shows one result of images processing of two-phase electrolysis processing conducted during 1.8 and 0 gravity level periods. It confirms that the bubble diameter is greater in the absence of gravity than in its presence. The bubble diameter increases with the intensity of current I and reaches its maximum value in the zero – gravity phase. The Fig. 7 shows that the formation and growth of bubbles depends on the applied current intensity.

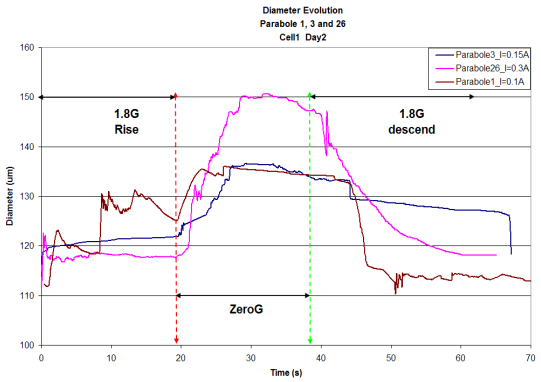

Fig. 7. Bubbles diameter evolution with current intensity

When the current intensity increases, the thickness of gas - film and the average bubble coverage Θ increases. Increasing the current intensity increases the number of active nucleation sites and even the production of bubbles, which increases the average coverage bubbles. The presence of the layer of bubbles along the electrode wall causes a decrease of the reactive surface area. The detachment of bubbles from the electrode wall produced an agitation in the liquid bulk which causes better transport of electroactive species. The presence of bubbles increases the electrolyte resistance which decreases the local electrical conductivity σ of electrolyte.

3. NUMERICAL METHODOLOGY

The analogy between mass and heat transfer allows defining the properties of mass transfer from those of heat transfer, for this reason we conducted a numerical simulation of heat exchange between the bubble and the liquid. It is considered that the deformation of the bubble is insignificant. We consider the bubble as a solid spherical particle. The study object is the numerical simulation of flow around an immobile spherical particle in 2D and 3D in an isotherm environment (Fig. 8).

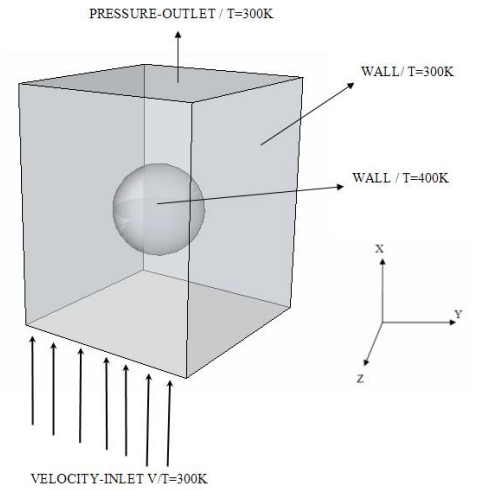

Fig. 8. Schematic representation of the problem geometry

The fluid and the particle properties and the cavity field dimensions are listed in the Table 2.

Table 2 Fluid, particle, and cavity properties

Cavity Height H(m)	Cavity Width d(m)	Particle Diameter (m)	Applied Velocity V(m/s)	Fluid Type	Fluid Density ρ(kg/m3)	Fluid Viscosity μ(kg/m.s)	Particle Temperature Tp(K)	Fluid Temperature T(K)
0.026	0.016	0.008	0.01 0.02 0.025 0.05 0.1	Water	1000	0.001	400	300

This work led to on laminar forced convection for and different imposed velocities to have Reynolds numbers ranging from 20 to 500. The hydrodynamics and heat transfer properties in the flow around the particle have been validated by comparing the results of numerical simulation with several experimental and numerical correlations for the average Nusselt number and the drag coefficient Cd find in the literature. The flow is governed by the Navier – Stokes and energy equations.
Mass continuity equation

$$\nabla.\vec{V} = 0 \tag{8}$$

Momentum equation

$$\rho\frac{\partial\vec{V}}{\partial t} + \rho(\vec{V}.\nabla)\vec{V} = -\nabla p + \vec{F} + \mu\nabla^2\vec{V} \tag{9}$$

With

$$F = F_D = \frac{C_D\pi d^2\rho V^2}{8}$$

Energy equation

$$\rho C_p\left[\frac{\partial T}{\partial t} + (\vec{V}.\nabla)T\right] = k\nabla^2 T \tag{10}$$

The drag coefficient C_D is calculated with the Morsi and Alexander (1972) correlation

$$C_D = a_1 + \frac{a_2}{\mathrm{Re}} + \frac{a_3}{\mathrm{Re}^2}$$

Where Re is the Reynolds number, a_1, a_2, a_3 are semi-empirical constants obtained with rigid spherical particles. This correlation was chosen by comparison with other correlation found in the literature.

Schiller and Neumann (1933) correlation

$$\begin{aligned} C_D &= \frac{24}{\mathrm{Re}}(1+0.15\mathrm{Re}^{0.687}) \quad \text{for} \quad \mathrm{Re} \le 1000 \\ C_D &= 0.44 \quad \text{for} \quad \mathrm{Re} \succ 1000 \end{aligned} \tag{11}$$

Schuh *et al.* (1989) correlation

$$C_D = \frac{24}{\mathrm{Re}}(1+0.15\mathrm{Re}^{0.687}) \quad \text{for} \quad \mathrm{Re} \le 200$$

$$C_D = \frac{24}{\mathrm{Re}}(0.914\mathrm{Re}^{0.282} + 0.135\mathrm{Re}) \quad \text{for} \quad 200 \le \mathrm{Re} \le 2500$$

For the interval of Reynolds number in this study, the difference between the three correlations is less than 4%. The result given in Fig. 9 allows validating the use of Morsi and Alexander (1972) correlation.

The Nusselt number Nu is calculated with the Ranz and Marshall (1952) correlation:

$$Nu = 2 + 0.6\mathrm{Re}^{0.5}\,\mathrm{Pr}^{1/3} \tag{13}$$

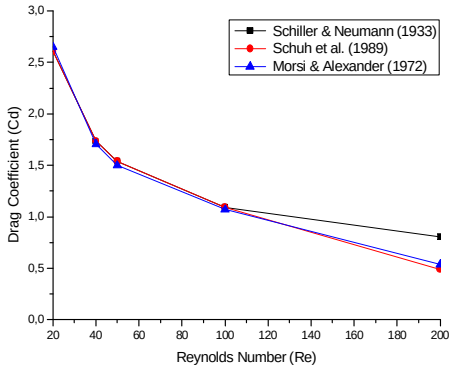

Fig. 9. Comparison of used drag coefficient correlation with the numerical correlations of Schiller and Neumann and Shuch and al.

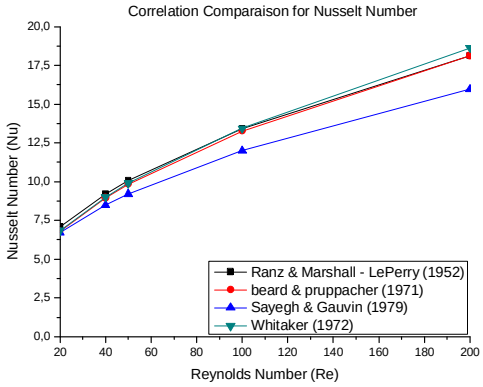

Fig. 10. Comparison of used Nuselt number correlation with the numerical correlation of Beard and Pruppacher, the experimental correlation of Witaker and the numerical correlation Sayegh and Gauvin.

Where Pr is the Prandlt number, this correlation was chosen by comparison with others correlations finding in the literature. The heat transfer analogue of the experimental mass transfer correlation presented by Beard and Pruppacher (1971) which is an excellent agreement with numerical results of Woo and Hamielec (1971) is

$$Nu = 1.56 + 0.616\,\mathrm{Re}^{0.5}\,\mathrm{Pr}^{1/3} \tag{14}$$

Another correlation is due to Witaker (1972) who found that the best fit to the experimental data is

$$Nu = 2 + (0.4\,\mathrm{Re}^{0.5} + 0.06\,\mathrm{Re}^{2/3})\,\mathrm{Pr}^{0.4} \tag{15}$$

Sayegh and Gauvin (1979) used numerical techniques to obtain:

$$Nu = 2 + 0.473\,\mathrm{Re}^{0.552}\,\mathrm{Pr}^{0.78}/\mathrm{Re}^{0.145} \tag{16}$$

The correlation of the Clift *et al.* (1978) based on available numerical solutions is

$$Nu = 1 + \left[1 + (\mathrm{Re}\,\mathrm{Pr})^{-1}\right]^{1/3} \mathrm{Re}^{0.41}\,\mathrm{Pr}^{1/3} \tag{17}$$

All of the obove-mentioned correlations in the range of Reynolds Number $20 \le \mathrm{Re} \le 200$, for this interval of Reynolds number, the gap between the five Nusselt number correlations is below 10%. The result given in Fig. 8 allows validating the use of Ranz and Marshall (1952). The choice of correlation for the Nusselt number and drag coefficient has been compared with the numerical results. The discrepancy between used Nusselt number and drag coefficient correlation and the numerical result.

4. Results and Discussions

4.1. Mesh and the Convergence Parameter

The laminar calculation was run with 3D solver using the triangular mesh (unstructured mesh) with mesh sizes of the order of 10^{-4} (Fig. 9). The run had converged when the residue reaches the maximum value of convergence (Fig. 11).

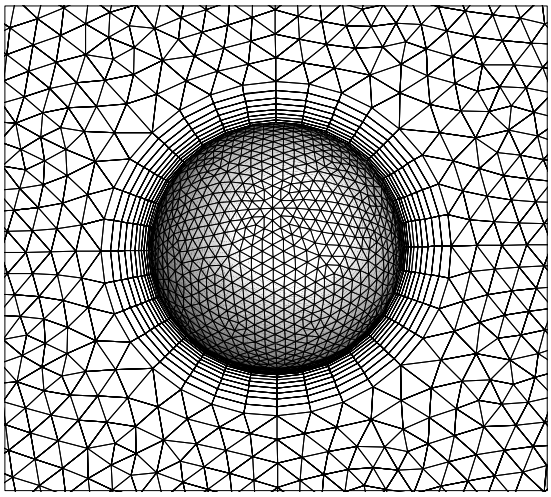

Fig. 11. bubble mesh

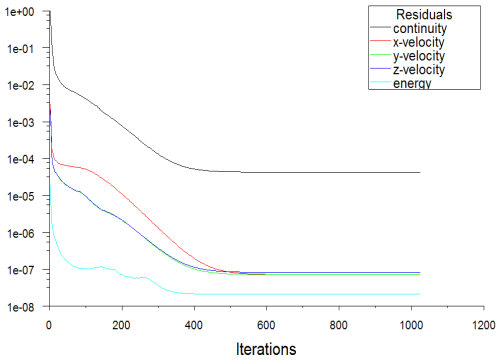

Fig. 12. Plot Convergence (maximal convergence)

Maximum convergence is reached when it is observed a plateau of velocity and mass residues.

4.2 Nusselt Number Modeling

To test the software in the Reynolds number range a run was performed for Re=20 to 200. The particle was located at the origine and had a diameter 0.001mm. The flow was in X direction with differents velocities (Table1). The test consists to compare the results

numerical simulation for the Nusselt number and drag coefficient with the theorical correlation mentioned in the last paragraph.

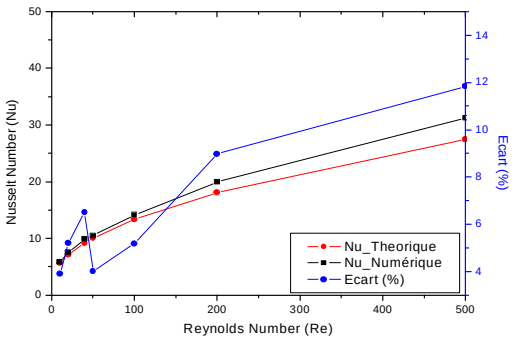

Fig. 13. Comparison between Nusselt number numericals and theoricals values

The difference between the numerical and the theorical value of Nusselt number is less than 9%. The choice of correlations is confirmed by this result. Figure 14 shows the local distribution of Nusselt number for Re =20 to 200 and Three different Prandlt number Pr=7, 20, 50 and 100.

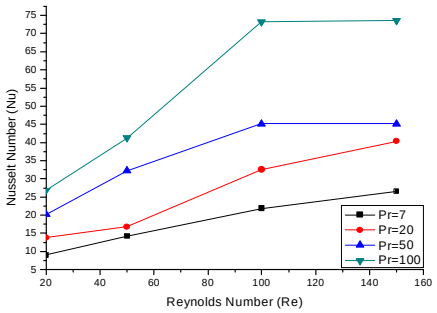

Fig. 14. Nusselt number distributions for flow over a spherical particle.

The thermal boundary layer becomes thinner leading higher heat transfer rates are the Reynolds number increases.

4.3 Velocity Fields

Figure 13 shows the velocity magnitude contours for a 1mm particle diameter for a Re =20; Pr=7 (a) and Re=150; Pr=7 (b).

When the inlet velocity increase (Re increase), the vortex was formed in the boundary layer zone and the heat exchange between particle and fluid increase. The calculation results allow the determination the influence of numerical condition of the velocity and the particle propriety in the heat transfer proprieties.

4. Conclusion

As it is shown in this work, the bubble scale calculation provides information in term of transfer which must be integrated at the macro reactor scale. The description of two-phase boundary layer at a boundary condition like an electrode remains of a great difficulty.

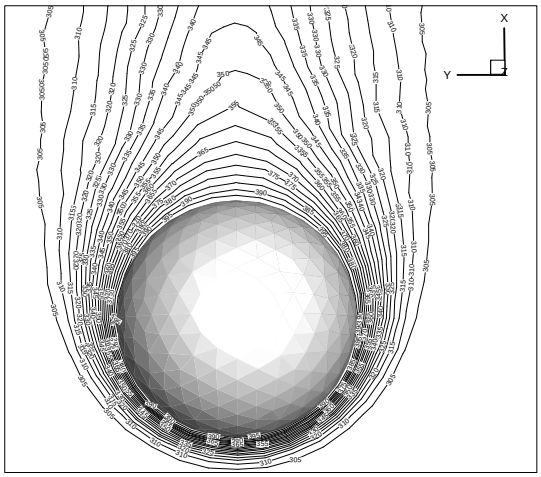

(a)

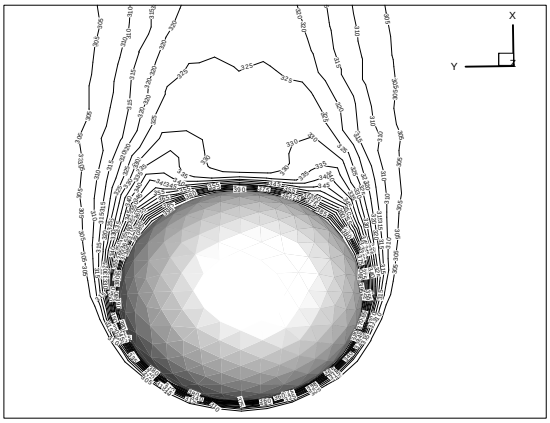

(b)

Fig. 15. Temperature contours for Re=20; Pr=7 (a) and Re=20; Pr=7 (b) d=0.001m.

References

Azumi, K., T. Mizuno, T. Akimoto and T. Ohmori (1999). *J. Electrochem. Soc.* 146, 3374.

Eigeldinger, J., and H. Vogt (2000). *Electrochimica Acta* 45(27), 4449-4456.

Gabrielli, C., F. Huet and R.P. Nogueira (2005). *Electrochimica Acta* 50(18), 3726-3736.

Janssen, L.J.J. and J.G. Hoogland (1970). *Electrochimica Acta* 15, 1020.

Janssen, L.J.J., C.W.M.P. Sillen, E. Barendrecht and S.J.D. Van Stralen (1984). *Electrochimica Acta* 29(5), 633-642.

Mandin, Ph., J. Hamburger, S. Bessou and G. Picard (2005). *Electrochimica Acta* 51(6), 1140-1156.

Mandin, Ph., H. Roustan, R. Wüthrich, J. Hamburger and G. Picard (2007). Simulation of Electrochemical Processes II. *Transactions on Engineering Sciences*, WIT Press, 73.

Mandin, Ph., A. Ait Aissa, H. Roustan, J. Hamburger and G. Picard (2008). *Chemical Engineering and Processing: Process intensification* 47, 1926-1932.

Matsushima, H., T. Nishida, Y. Konishi, Y. Fukunaka, Y. Ito and K. Kuribayashi (2003). *Electrochimica Acta* 48(28), 4119-4125.

Matsushima, H., Y. Fukunaka and K. Kuribayashi (2006). *Electrochimica Acta* 51(20), 4190-4198.

Vogt, H. and Ö. Aras, R.J. (2004). *Balzer International Journal of Heat and Mass Transfer* 47(4), 787-795.

Vogt, H. and R.J. Balzer (2005). *Electrochimica Acta* 50(10), 2073-2079.

Wüthrich, R, L.A. Hof, A. Lal, K. Fujisaki, H. Bleuler, Ph. Mandin and G. Picard (2005). *J. of Micromech. Microeng.* 15, 268-275.